SUPPLEMENTARY INFORMATION

Synergistic construction of defect-rich nanozymes via montmorillonite support loading and iron doping for enhanced peroxidase-like activity

Wenjie Qu[1], Xiaorong Yang[1], Feng Feng[1], Yihe Zhang[1] Wangshu Tong[1]

Engineering Research Center of Ministry of Education for Geological Carbon Storage and Low Carbon Utilization of Resources, Beijing Key Laboratory of Materials Utilization of Nonmetallic Minerals and Solid Wastes, National Laboratory of Mineral Materials, School of Materials Science and Technology, China University of Geosciences (Beijing), Beijing 100083, China

EXPERIMENTAL SECTION

Synthesis of FMM, MM, FM and MoS_2.

FMM NPs were prepared by our previously developed method.[1] Specifically, montmorillonite solution (1mg/mL) were prepared and then dispersed by ultrasound (400 W) for 30 minutes. Then, CH_4N_2S(15mmol), $Fe(NO_3)_3$•$9H_2O$(0.349mmol) and $(NH_3)_2MoO_4$•$4H_2O$(0.449mmol) were dissolved in montmorillonite solution (60mL), and continued stirring for 60 min. Subsequently, the mixture was transferred into a Teflon-lined autoclave (100mL) and heated at 200℃ for 24h. After cooling down to room temperature, the product was washed by deionized water and ethanol for several times and collected by centrifugation (8000 rpm). Finaly, the obtained FMM NPs were dried in a vacuum oven at 60℃ for 4 h. Similarly, MoS_2, FM and MM were synthesized via the same method, however, by omitting both MMT and $Fe(NO_3)_3$•$9H_2O$ (0.349mmol), MMT, or $Fe(NO_3)_3$•$9H_2O$ (0.349mmol) respectively.

Characterizations

The surface morphologies and structure of prepared nanozymes were characterized by scanning electron microscope (SEM) on a ZEISS Sigma 300. The method of Brunauer-Emmett-Teller (BET) specific surface area and pore distribution was determined using a Quantachrome nova 2000. X-Ray Diffraction (XRD) patterns was measured on an EQUINOX 3000 using Cu Kα radiation. X-ray photoelectron spectroscopy (XPS) patterns were acquired using Thermo Scientific K-Alpha to analyze the electron transfer. The Raman spectra were measured via spectrometer (RTS2-DZ-A). The UV-7600 was used for recording the absorbance of color reaction. Coupled Plasma-Optical Emission Spectrometry (ICP-OES) measurements were performed on a Thermo Scientific iACP 6000. In situ ATR-FTIR spectra was measured on a Bruke TENSOR II.

Evaluation of Peroxidase (POD) - like activity

TMB (3,3,5,5-tetramethylbenzidine) oxidation assay was carried out to evaluate the POD-like activity of samples, as the oxidized TMB (oxTMB) showing maxium

adsorption at 652nm. Briefly, 1.25μg mL^{-1} of the sample was mixed with 1 M H_2O_2 and 2.08 mM TMB sodium acetate buffer (pH=3.6). After co-incubation of the mixture, the relevant absorbance scans about time were recorded. For kinetic assay of FMM (5 ug mL^{-1}) and FM (10 ug mL^{-1}) the experiments were carried out in 2mL of HAc-NaAc buffer (pH 4.0), 2.08 mM TMB, and a series of concentrations of H_2O_2 range from 0 to 10mM, or 1 M H_2O_2, and a series of concentrations of TMB range from 0 to 12.48 mM. Similarly, for kinetic assay of MoS_2 (25 ug mL^{-1}) and MM (10 ug mL^{-1}) the experiments were carried out in 2mL of HAc-NaAc buffer (pH 4.0), 2.08 mM TMB, and a series of concentrations of H_2O_2 range from 0 to 125 mM, or 1 M H_2O_2, and a series of concentrations of TMB range from 0 to 4.16 mM. The content of Mo element was measured by ICP-OES. All experiments were repeated three times.

Bacterial culture and antibacterial experiments.

The antibacterial effect of nanozymes was determined using the plate counting method. First, *E. coli* and *S. aureus* were cultured in nutrient broth at 37 °C in an incubator shaker (120 rpm) for 24 h. Then, the bacteria were diluted in PBS buffer (pH 7.2). obtaining final concentration of *E. coli* and *S. aureus* were 1~1.5 $\times 10^8$ CFU mL^{-1}, respectively. The initial bacteria solution was diluted to a concentration of around 1 $\times$ 10^5 CFU mL^{-1} or lower for the antibacterial experiments. Next, 100 μL of bacteria solution was then mixed with nanozyme and H_2O_2 (1 mM for E. coli and 0.1 mM for S. aureus) in 1mL PBS buffer (pH 4.3). The mixed solution was incubated for 1 h at 37 °C in incubator shaker (80 rpm). Then, 200 μL of the mixture was homogeneously mixed on solid agar medium before solidification and incubated at 37 °C for 24 h. Finally, optical photographs were then taken as well as the antibacterial rate was calculated.

In situ ATR-FTIR Spectroscopy

H_2O_2 evolution process over FMM and MM surface were recorded by using a Bruke TENSOR II. First, a dense film was prepared on the surface of the sample table using the material.[2] Subsequently, a buffer solution with pH = 4 was added as a control.

Finally, 20 microliters of a 10 mM H_2O_2 solution at pH 4 were added to initiate the reaction.

Calculation details

All calculations were conducted using the Vienna Ab Initio Simulation Package with the projector augmented wave method in the framework of density functional theory (DFT). The generalized gradient approximation (GGA) method with the Perdew-Burke-Ernzerhof (PBE) functional was applied to describe the exchange and correlation energy. The DFT-D3 method of Grimme et al. was utilized to calculate the van der Waals correction.[3] The plane-wave cut-off energy was set to 400 eV, and the convergence tolerance for residual force and energy on each atom during structure relaxation were set to 0.02 eV/Å and 10^{-5} eV, respectively.[4] During the search of transition states, a lower force threshold of 0.05 eV/Å was used. A model of a 4 × 4 supercell and a >15 Å vacuum thicknesses to avoid interaction between the layers. A Monkhorst-Pack *k*-point sampling of 3 × 3 × 1 was adopted.

Gibbs free energies were calculated from DFT total energies corrected by zero-point energy (*ZPE*), and entropy (*TS*), according to the expression.

$$G = E_{DFT} + E_{ZPE} - TS + \Delta G_{pH}$$

Where *E*, *ZPE*, *T* and *S* represent the DFT calculated energy, zero-point energy, temperature (298.15K), and vibrational entropy, respectively. The effect of basic/acidic condition (pH effect) on thermodynamics is described by $\Delta G_{pH} = -k_B T ln[H^+]$.[5] The thermodynamic correction was carried out by using the VASPKIT code.[6] Structural and charge density visualization were conducted utilizing the VESTA software.[7]

PARTIAL RESULTS AND DISCUSSION

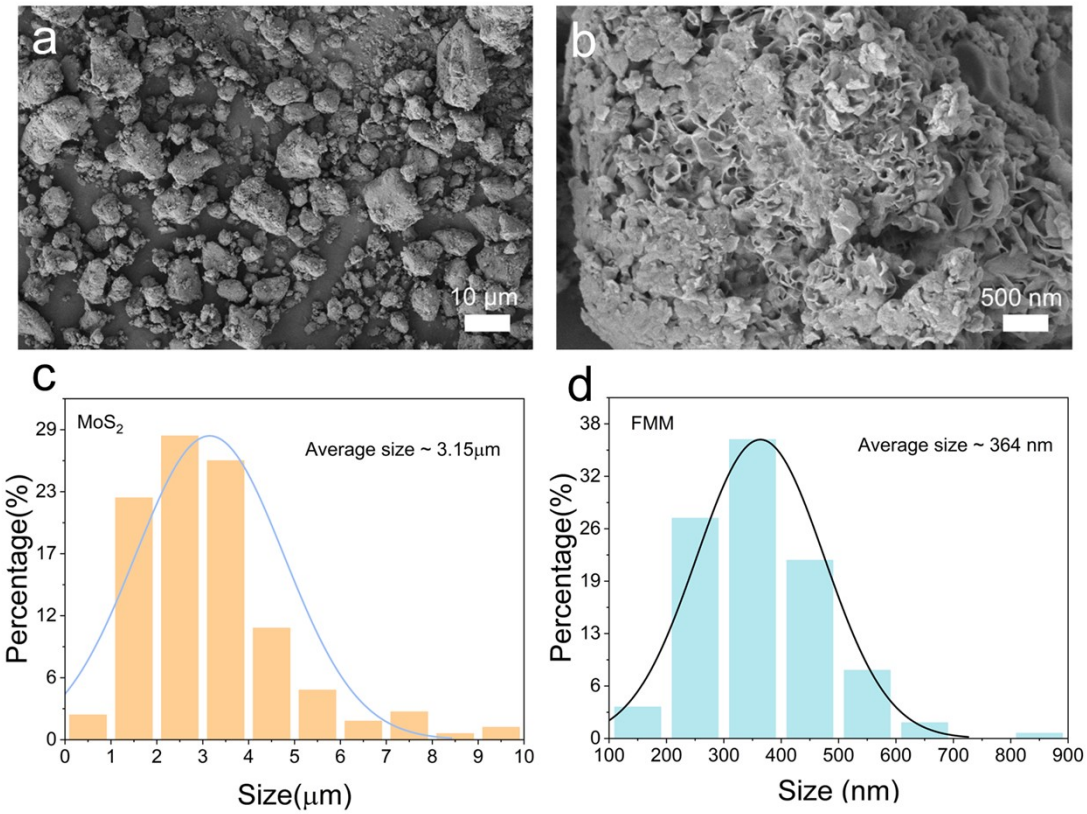

Figure S1. (a, b) SEM image of FM. Particle-size distributions of FMM (c) and MM (d).

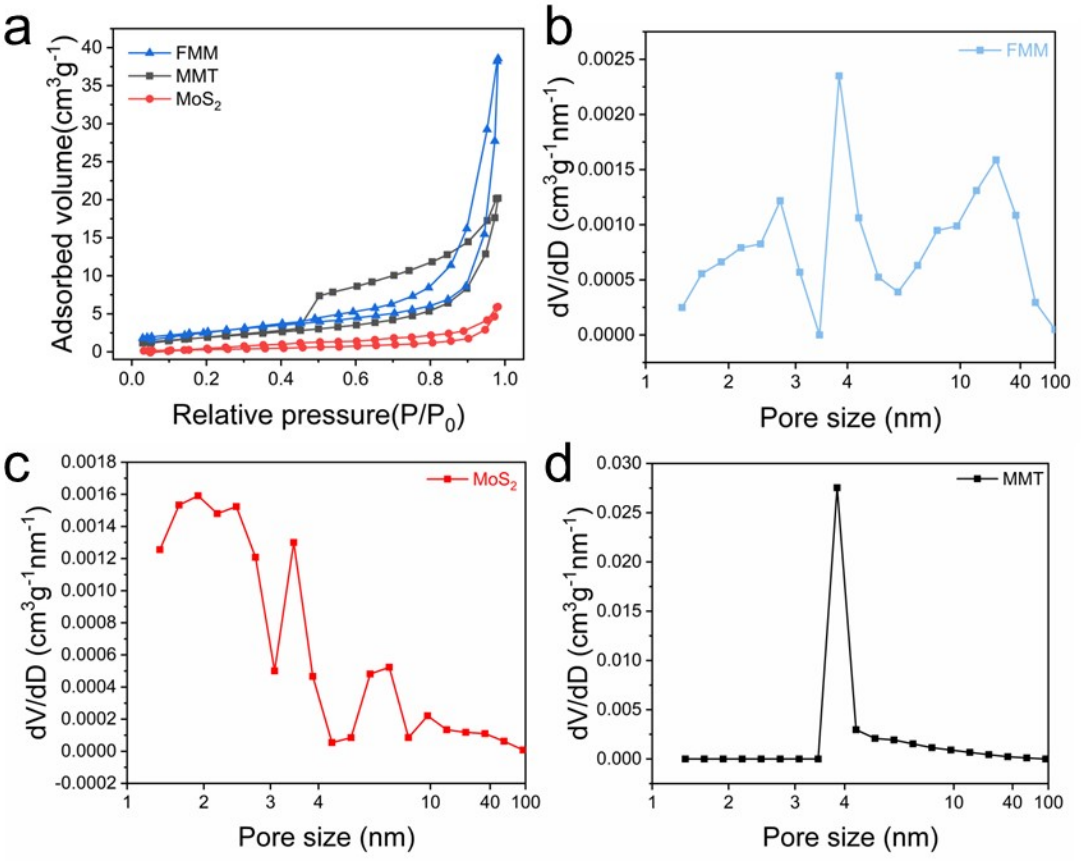

Figure S2. (a) BET isotherm of FMM, MMT, and MoS_2. Pore size distribution curve of FMM (b), MoS2 (c), and MMT (d).

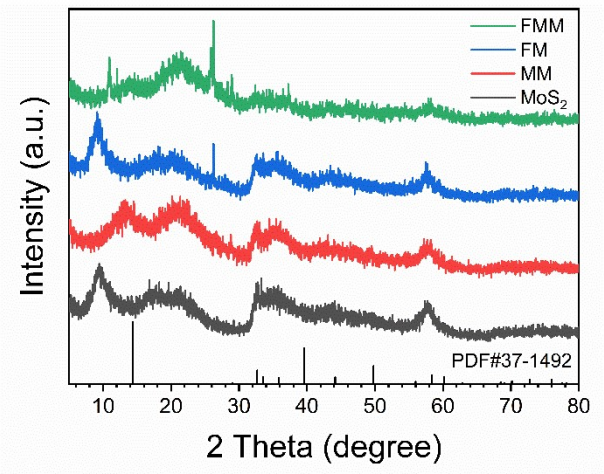

Figure S3. XRD of FMM, FM, MM, and MoS_2.

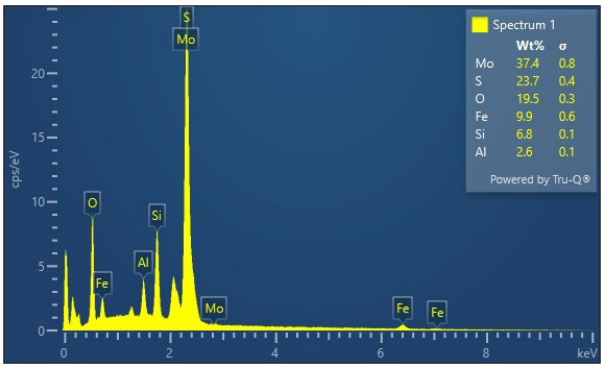

106 Figure S4. EDS of FMM

107

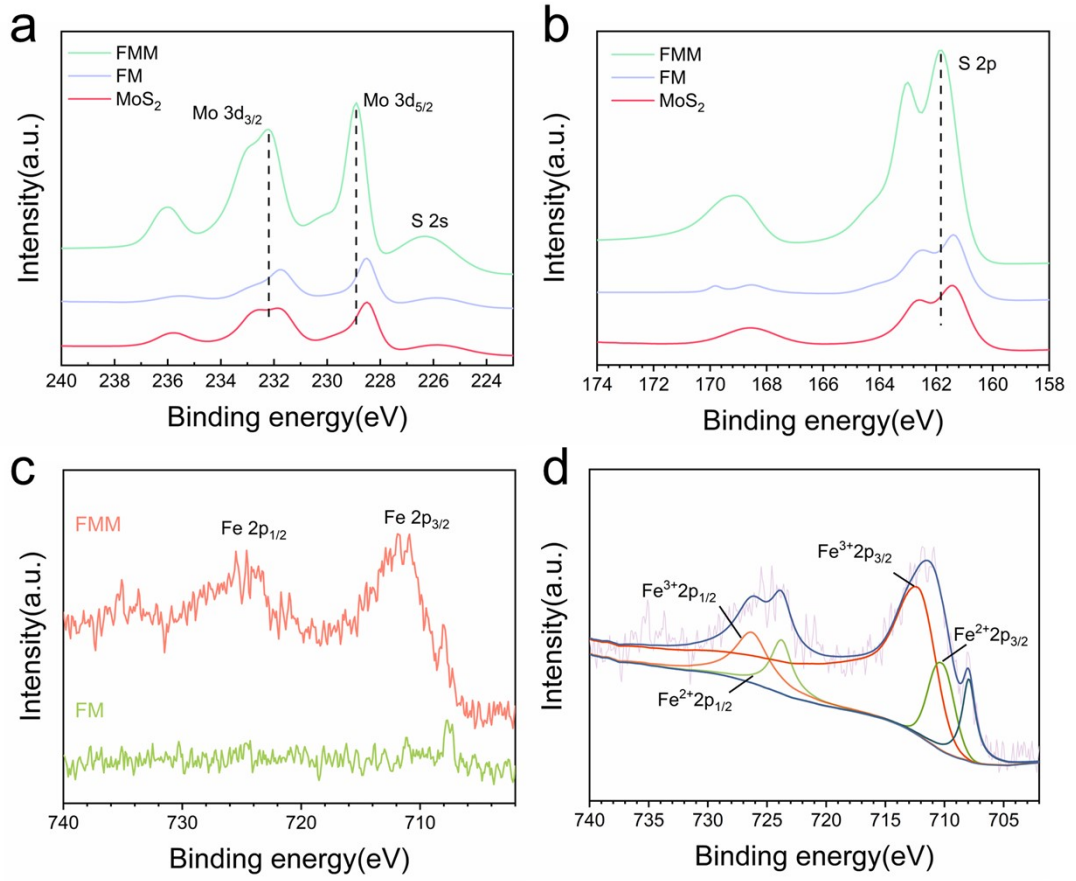

Figure S5. (a) High-resolution Mo 3d XPS spectra of FMM, FM, and MoS_2. (B) High-resolution S 2P XPS spectra of FMM, FM, and MoS_2. (c) High-resolution Fe 2p XPS spectra of FMM and FM.(d) Fe 2p XPS spectra of FMM.

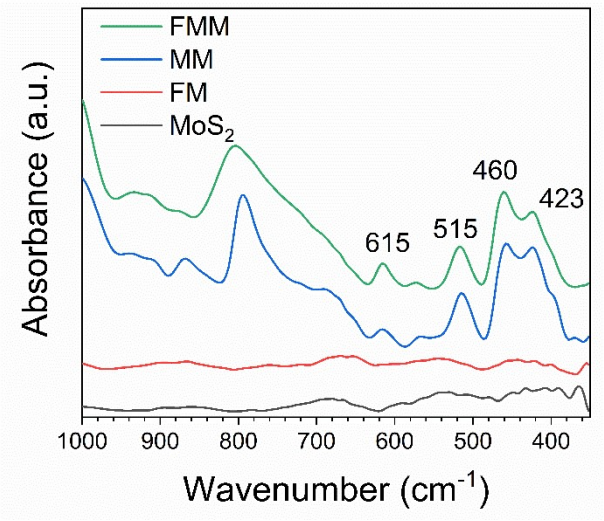

Figure S6. ATR-FTIR of FMM, MM, FM, and MoS_2.

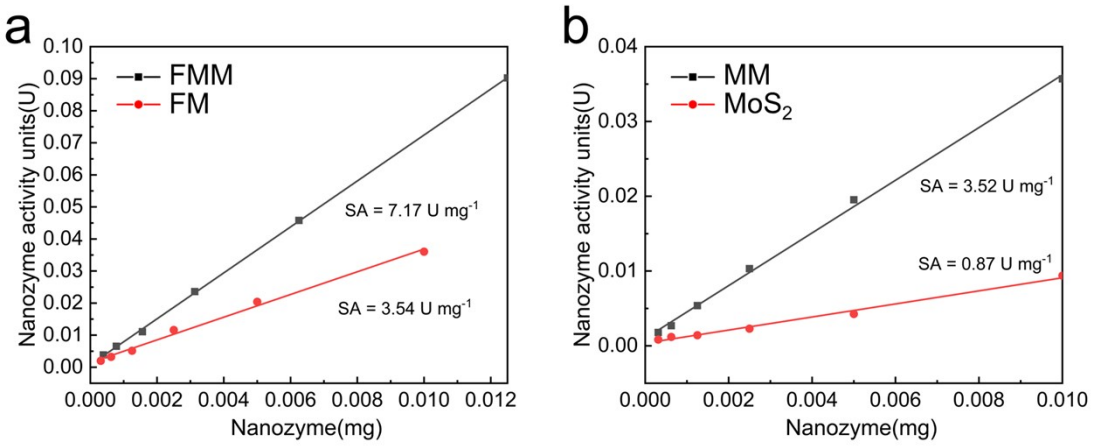

Figure S7. specific activity of FMM, FM, MM and MoS_2.

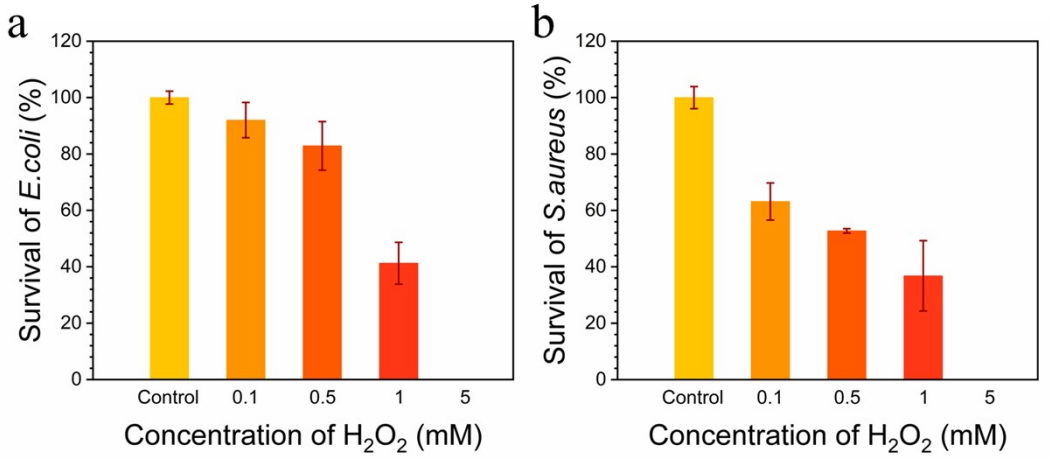

Figure S8. (a) *E. coli* and (b) *S. aureus* after coincubation with different concentrations of H_2O_2. Error bars were taken from three parallel tests per group.

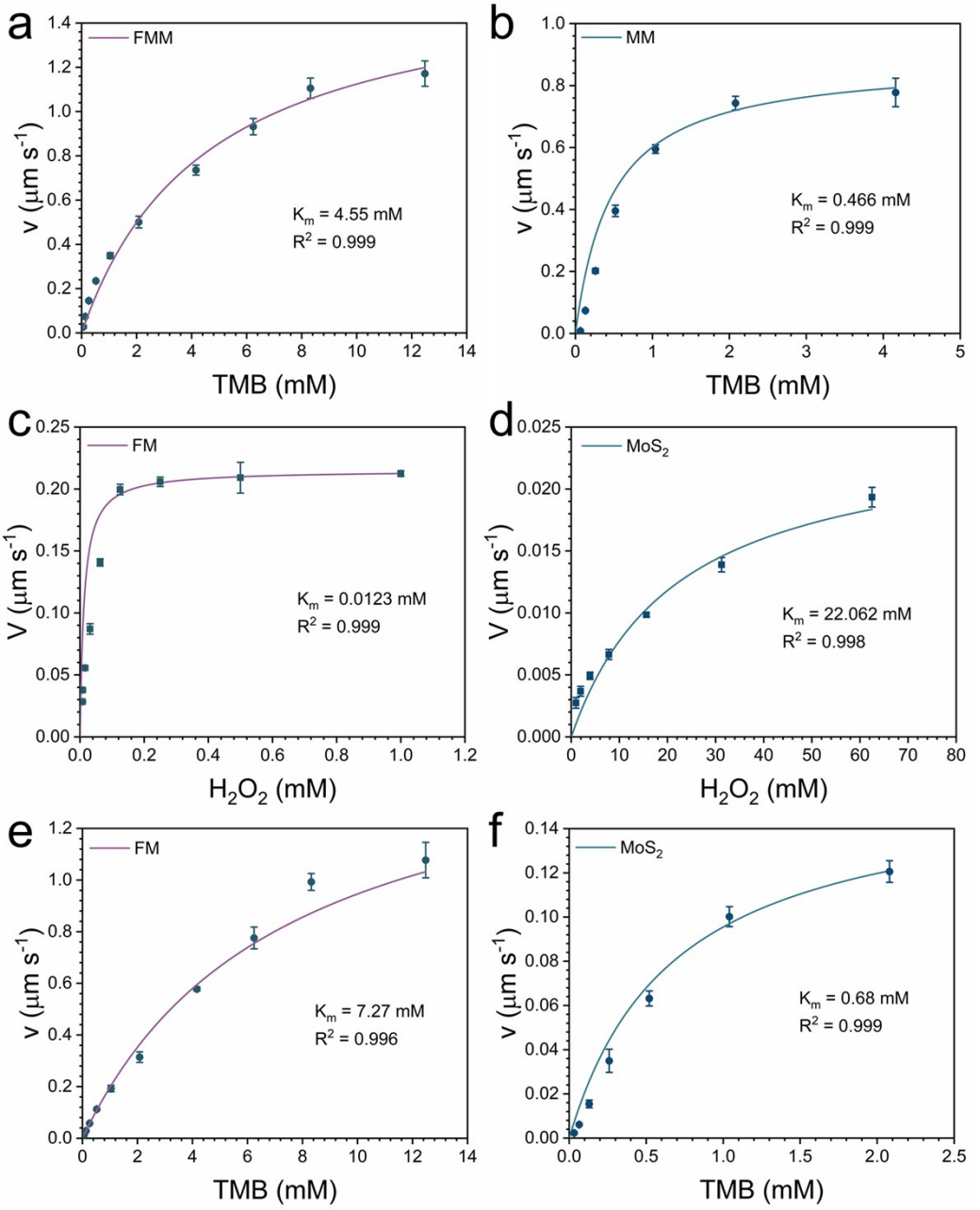

Figure S9. Steady-state kinetic assay. FMM (a) and MM (b) with TMB as substrate. FM (c) and MoS_2 (d) with H_2O_2 as substrate. FM (e) and MoS_2 (f) with TMB as substrate.

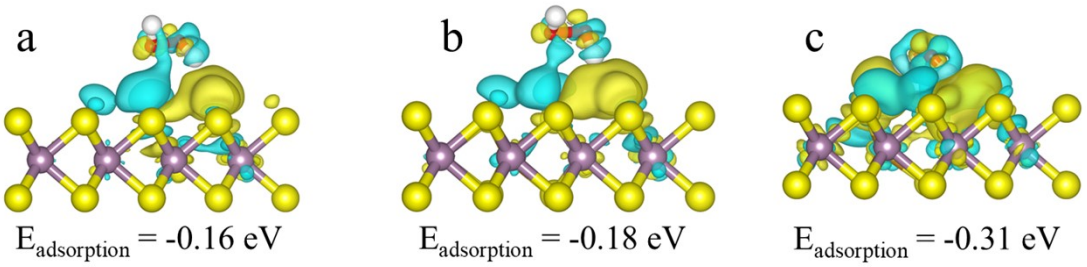

Figure S10. Adsorption energy of H_2O_2 at MoS_2 (a), FM (b), and Sv site of FM (c).

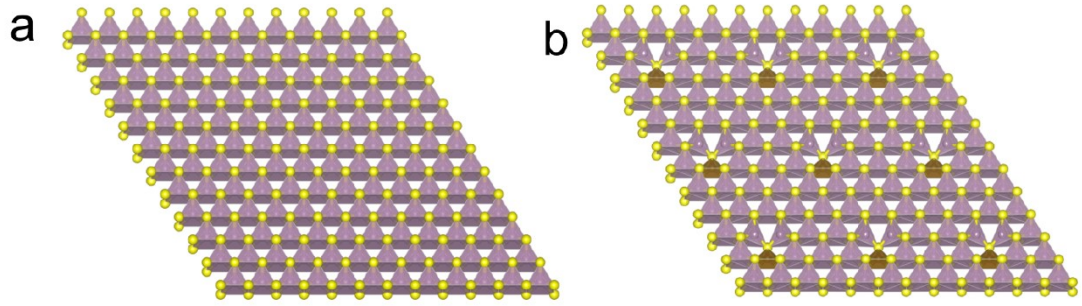

Figure S11 Structural model diagram of MoS_2 (a), and Sv site in FM (b).

It can be observed that there is a one-to-one correspondence between iron doping and sulfur vacancies. In the Sv site of FM, the active center is composed of non-vacant Mo atoms and sulfur vacancies.

$$K_{cat} = \frac{V_{max}}{[E]} = \frac{V_{non-vacant} + V_{Sv\ site}}{[E]_{non-vacant} + [E]_{Sv\ site}} = \frac{V_{non-vacant} + V_{Sv\ site}}{[E]_{Mo} - [E]_{Fe}}$$

$$[E]_{non-vacant} = [E]_{Mo} - 2 \times [E]_{Fe}$$

$$[E]_{Sv\ site} = [E]_{Fe}$$

Here, $[E]_{Mo}$ and $[E]_{Fe}$ were measured using ICP-OES. V_{max} and K_{cat} were determined through steady-state kinetic measurements.

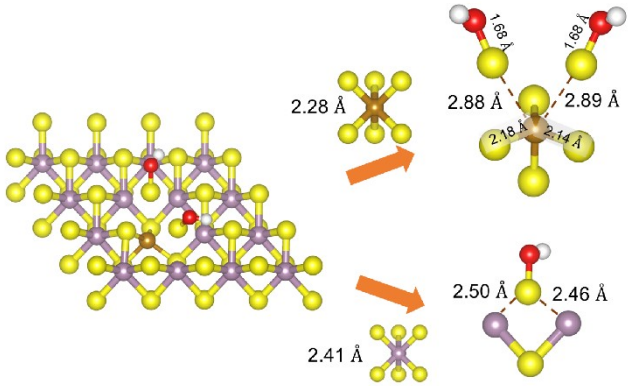

We further calculated the reaction of H_2O_2 at the Fe sites in FM and found that, during the second step where H_2O_2 decomposes into two *OH species, the S atom near the Fe site is pushed away from both the Fe and Mo atoms under the influence of *OH, facilitating the formation of sulfur vacancies. This result further demonstrates that the primary reason for the enhanced activity in Fe-doped MoS_2 is the generation of sulfur vacancies.

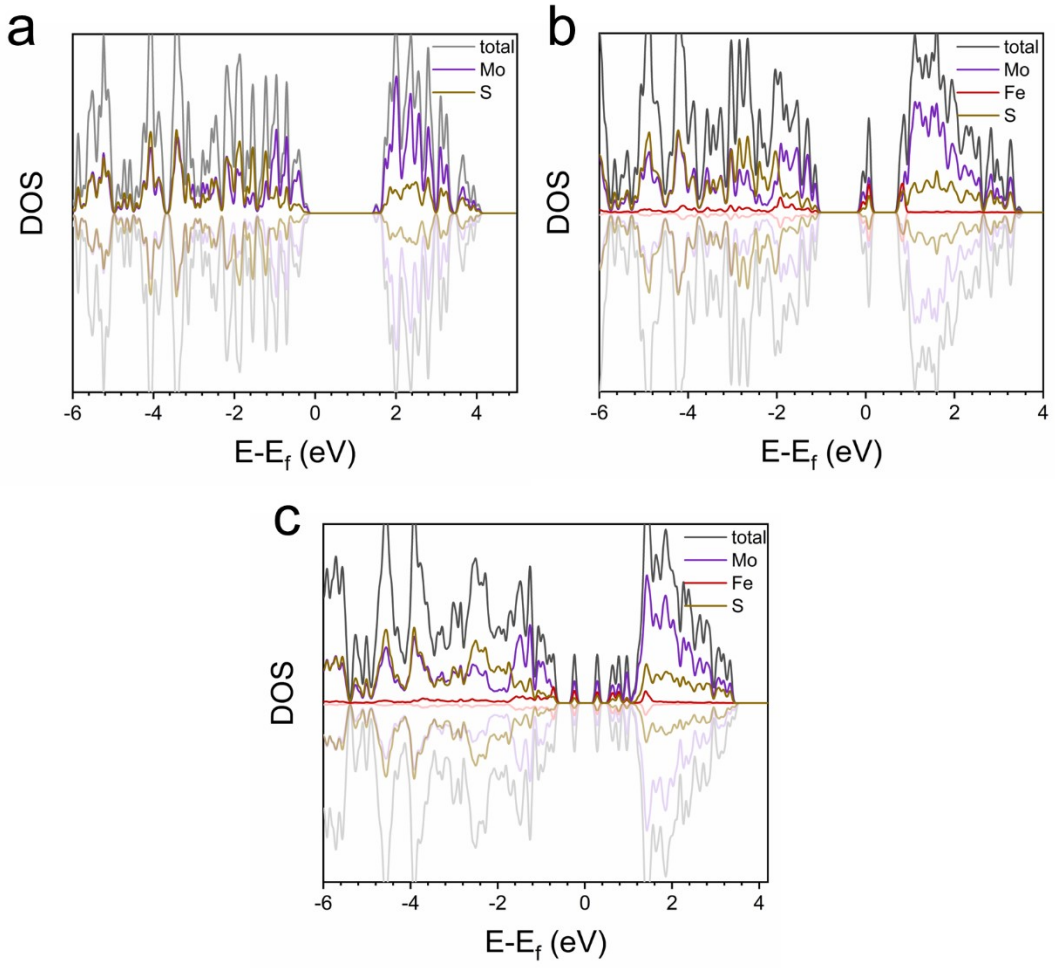

Figure S12 DOS of MoS2 (a), Fe-doped MoS_2 (b) and Sv site in FM (c).

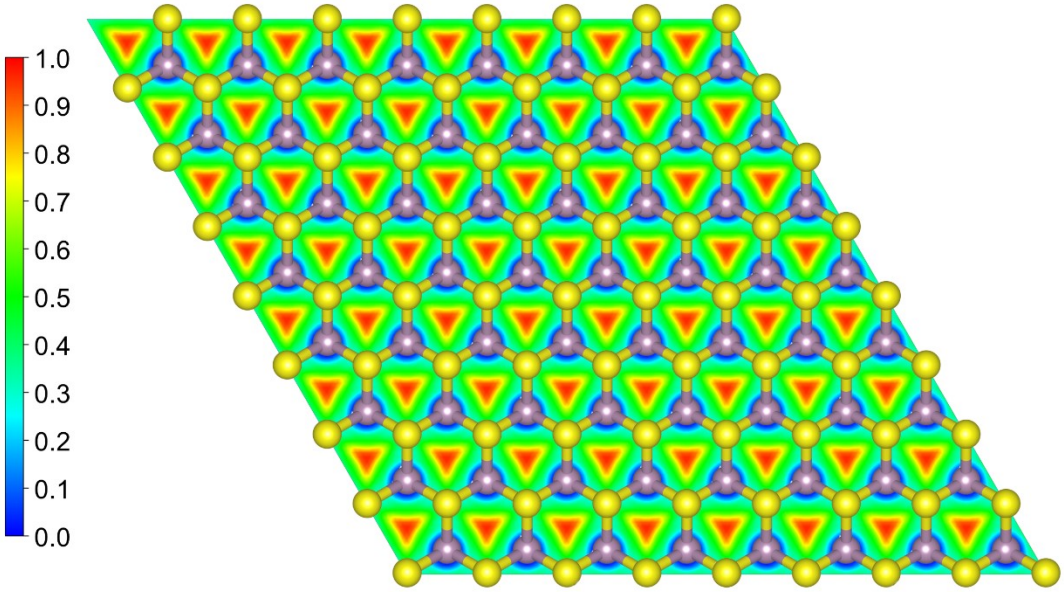

Figure S13 Electron Localization Function of MoS_2.

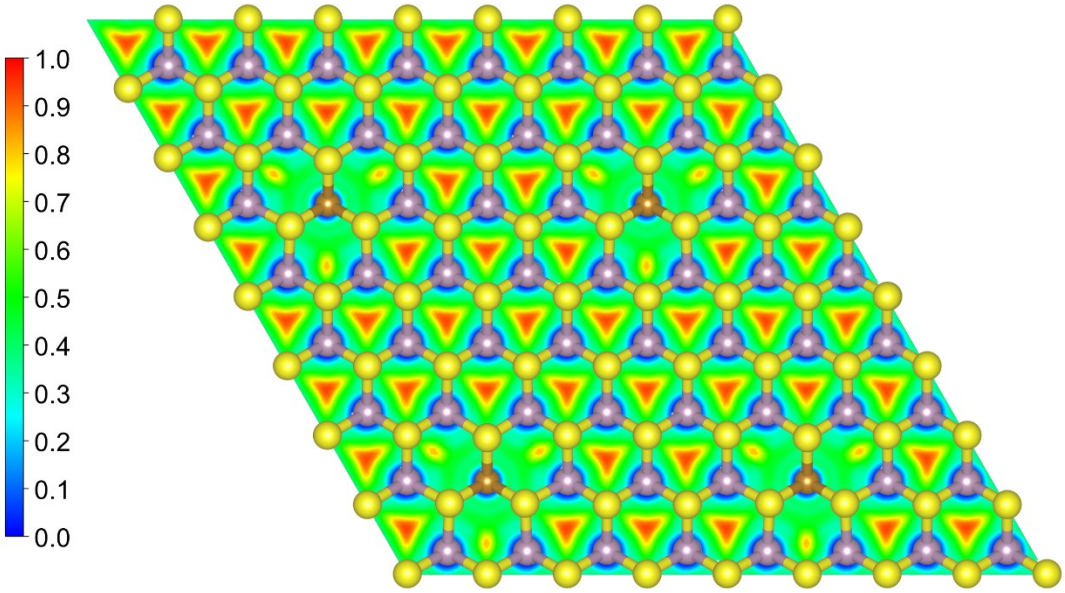

Figure S14 Electron Localization Function of Fe-doped MoS_2.

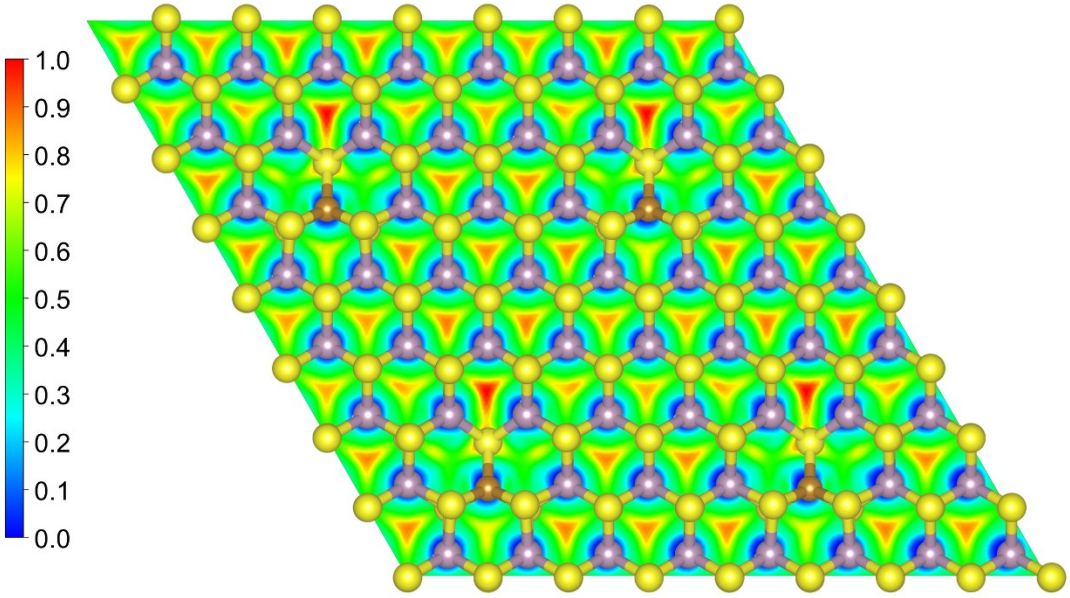

Figure S15 Electron Localization Function of Sv site in FM.

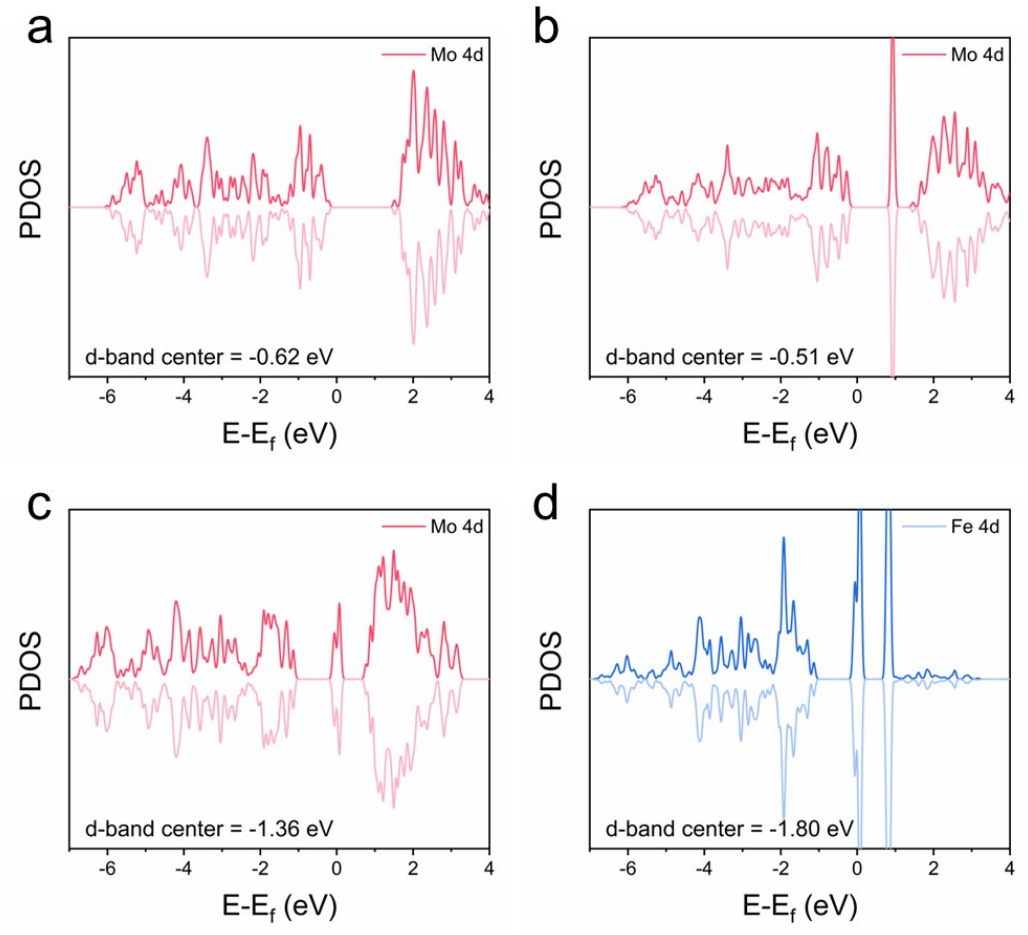

Figure S16. The calculated PDOS and Mo d-band center of MoS_2 (a), Sv site of MoS_2 (b), and Fe doping MoS_2 (c). The calculated PDOS and Fe d-band center of Fe doping MoS_2 (d).

In MoS_2, the formation of sulfur vacancies is challenging under standard conditions due to its structural stability, which is consistent with its relatively high d-band center. In Fe-doped MoS_2, the Mo atoms near the Fe doping sites exhibit an even higher d-band center, further demonstrating the critical role of Mo in the catalytic process.

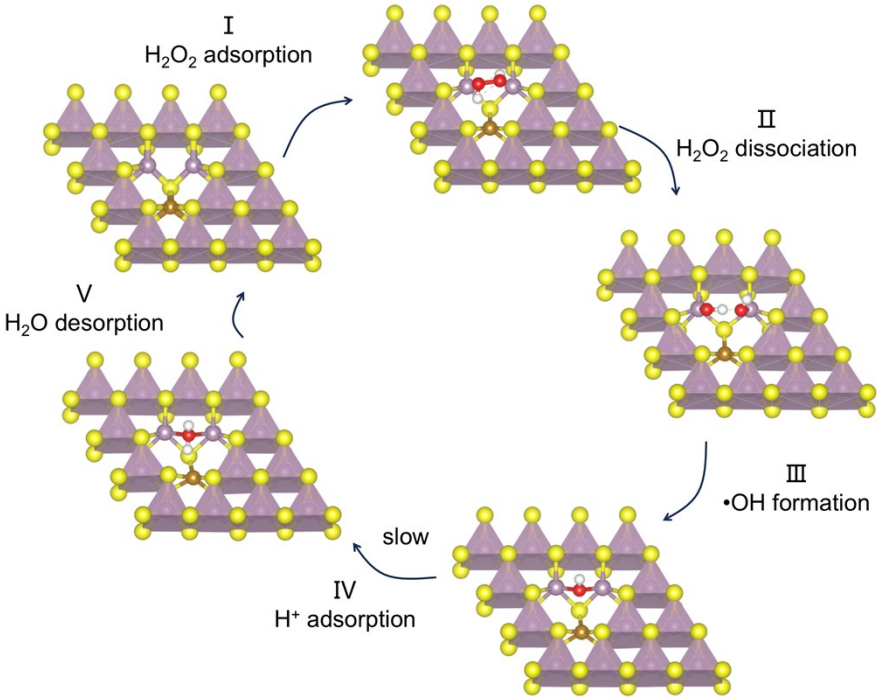

Figure S17. Schematic diagram of the reaction process of Sv site of FM.

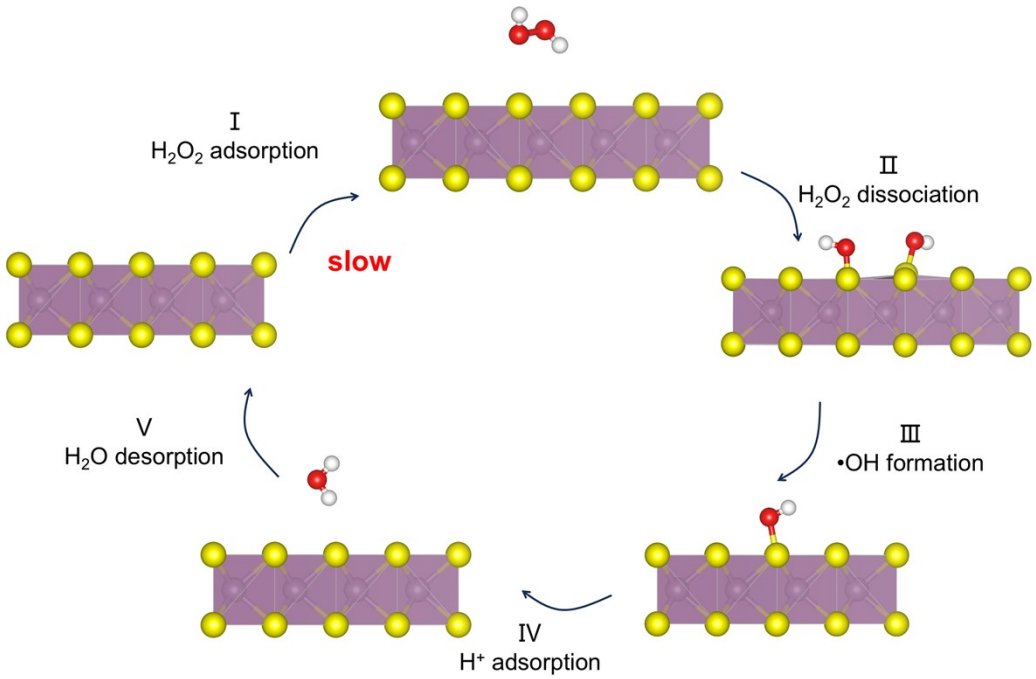

173

174 Figure S18. Schematic diagram of the reaction process of MoS_2.

175

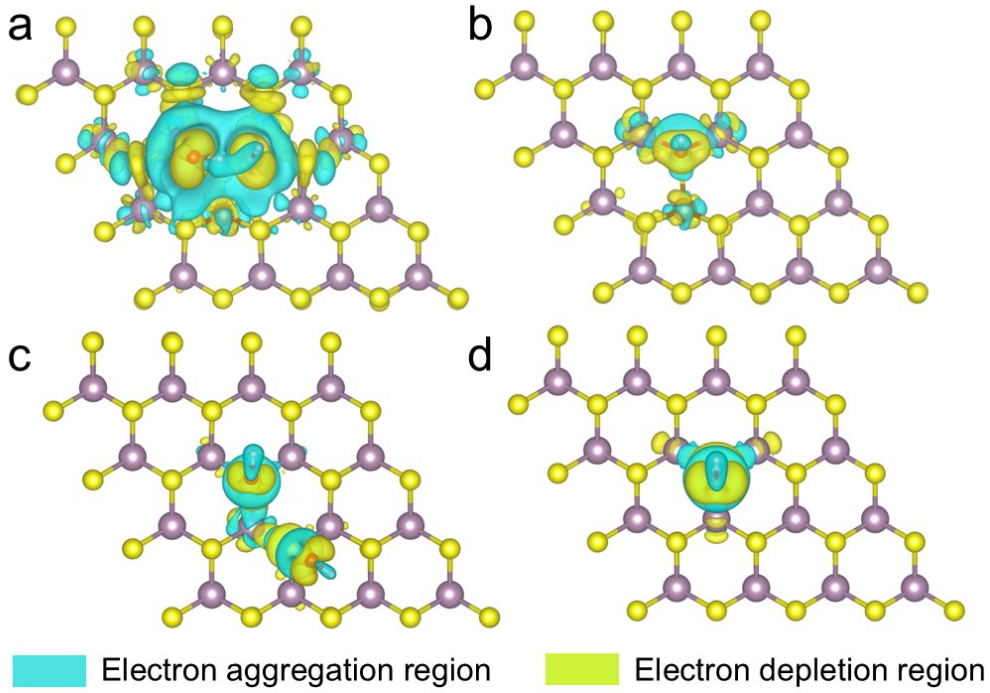

Figure S19. Top view of charge density difference of 2*OH or *OH on Sv site in FM (a, b) and MoS_2 (c, b), respectively.

Nanozyme	[E](M)	Substrates	K_M(mM)	V_{max}(mM s^{-1})	K_{cat}(s^{-1})	K_{cat}/K_M (mM^{-1} s^{-1})
FMM	2.51×10^{-5}	H_2O_2	0.038	0.225	8.97×10^{-3}	0.23
		TMB	4.55	1.64	0.065	0.014
MM	4.47×10^{-5}	H_2O_2	10.77	0.0786	1.76×10^{-3}	1.63×10^{-4}
		TMB	0.466	0.882	0.020	0.042
FM	4.53×10^{-5}	H_2O_2	0.0123	0.215	4.74×10^{-3}	0.385
		TMB	7.27	1.63	0.036	4.94×10^{-3}
MoS_2	9.55×10^{-5}	H_2O_2	22	0.025	2.62×10^{-4}	1.19×10^{-5}
		TMB	0.68	0.16	1.68×10^{-3}	2.46×10^{-3}

Table S1

Comparison of kinetics for FMM, MM, FM, and MoS_2. E is the molar concentration of Sv sites of FMM and FM and Mo sites of MoS_2, measured by inductively coupled plasma optical emission spectrometry (ICP-OES). K_m is the Michaelis-Menten constant. V_{max} is the maximal reaction velocity. K_{cat} is the catalytic rate constant. The value of K_{cat}/K_M represents catalytic efficiency.

Table S2

Nanozyme	Element	Content (%)	Concentration (mol L^{-1})
FMM	Mo	48.124	2.51×10^{-5}
	Fe	0.076	6.79×10^{-8}
FM	Mo	43.504	4.53×10^{-5}
	Fe	0.429	7.68×10^{-7}
MM	Mo	42.870	4.47×10^{-5}
MoS_2	Mo	36.641	9.55×10^{-5}

The element content in each material obtained by ICP test.

Reference

1. F. Feng, Y. Zhang, X. Zhang, B. Mu, J. Zhang, W. Qu, W. Tong, M. Liang, Q. An, Z. Guo and L. Zhao, *Nano Research*, 2024, **17**, 7415-7426.
2. C. Ling, X. Liu, H. Li, X. Wang, H. Gu, K. Wei, M. Li, Y. Shi, H. Ben, G. Zhan, C. Liang, W. Shen, Y. Li, J. Zhao and L. Zhang, *Angewandte Chemie International Edition*, 2022, **61**, e202200670.
3. S. Grimme, S. Ehrlich and L. Goerigk, *Journal of Computational Chemistry*, 2011, **32**, 1456-1465.
4. P. E. Blöchl, *Physical Review B*, 1994, **50**, 17953-17979.
5. A. Han, X. Wang, K. Tang, Z. Zhang, C. Ye, K. Kong, H. Hu, L. Zheng, P. Jiang, C. Zhao, Q. Zhang, D. Wang and Y. Li, *Angewandte Chemie International Edition*, 2021, **60**, 19262-19271.
6. V. Wang, N. Xu, J.-C. Liu, G. Tang and W.-T. Geng, *Computer Physics Communications*, 2021, **267**, 108033.
7. K. Momma and F. Izumi, *Journal of Applied Crystallography*, 2011, **44**, 1272-1276.